Biosensors and Bioelectronics 155 (2020) 112114

Contents lists available at ScienceDirect

Biosensors and Bioelectronics

journal homepage: http://www.elsevier.com/locate/bios

Niobium-doped TiS_2: Formation of TiS_3 nanobelts and their effects in enzymatic biosensors

Nasuha Rohaizad [a], Carmen C. Mayorga-Martinez [b], Zdeněk Sofer [b], Richard D. Webster [c], Martin Pumera [b,d,e,f,*]

[a] NTU Institute for Health Technologies, Interdisciplinary Graduate School, Nanyang Technological University, Singapore
[b] Center for Advanced Functional Nanorobots, Department of Inorganic Chemistry, University of Chemistry and Technology Prague, Czech Republic
[c] Division of Chemistry & Biological Chemistry, School of Physical and Mathematical Sciences, Nanyang Technological University, Singapore
[d] Department of Chemical and Biomolecular Engineering, Yonsei University, 50 Yonsei-ro, Seodaemun-gu, Seoul, 03722, South Korea
[e] Department of Medical Research, China Medical University Hospital, China Medical University, No. 91 Hsueh-Shih Road, Taichung, Taiwan
[f] Future Energy and Innovation Lab, Central European Institute of Technology, Brno University of Technology, Purkyňova 656/123, Brno, CZ-616 00, Czech Republic

ARTICLE INFO

Keywords:
Transition metal dichalcogenides
Layered
Metal doping
Electrochemistry
Second generation glucose biosensor

ABSTRACT

There is an assortment of layered transition metal dichalcogenides (TMDs), about 40 reported compounds, each with its unique polymorph and properties. Group 4 TMD, titanium disulfide (TiS_2), possess high electronic conductivity and light weight amongst other attractive features. In consideration for electrochemical and thermoelectrical applications, doping is a promising approach to enhance its practicability. The introduction of foreign atoms or compositional variance may improve existing properties or grant access to new ones. Moving away from the more intensively studied and successfully doped group 6 MoS_2 and WS_2, TiS_2 is doped with varying levels of niobium (Nb) via controlled heating of stoichiometric amounts to yield $Ti_{1-x}Nb_xS_2$ where x = 0.05, 0.1, 0.2. Structural effects are discussed together with two doping parameters, nature and concentration of dopant. Characterisation data reveal retention of 1T-phase polymorph despite formation of TiS_3 nanobelts upon doping. Fundamental electrochemical properties such as heterogenous electron transfer rates and its charge transfer resistance are compared amongst the materials of interest. A selective and sensitive 2nd generation electrochemical biosensor is prepared using $Ti_{0.95}Nb_{0.05}S_2$/GOx/GTA since it is the most superior material in glucose detection.

1. Introduction

Two-dimensional (2D) materials are classically represented by graphene. Undoubtedly so as it was the first in its class to be successfully isolated in 2004 along with a combination of enthralling properties reported, and again first to enter the market (Novoselov, 2004) (Geim and Novoselov, 2007) (Nat. Mater. 2019). A roadmap has been laid out, with ambitions that laboratories discoveries would transform into real applications and products (Ferrari et al., 2015). Following the reignited interest in graphene, transition metal dichalcogenides (TMDs) is another group of 2D materials that has been pursued. Its research has well-progressed and contemporarily riding the waves of printing (Rowley-Neale et al., 2017; Mcmanus et al., 2017; Hu et al., 2018; Higgins et al., 2018) and flexible (Singh et al., 2019; Zhang et al., 2019; Velusamy et al., 2015; Cheng et al., 2014) technologies. Apart from dimensionality, one attractive aspect of TMDs is elemental composition. There are about 40 layered compounds in the library of TMDs (Wilson and Yoffe, 1969), of varying transition metal or chalcogen component, showcasing diverse polymorphs, properties and versatile chemistry (Chhowalla et al., 2013; Chia and Pumera, 2018). Doping is a feasible strategy to expand the collection of compounds, improving old properties or accessing new ones (Tedstone et al., 2016; Luo et al., 2019).

Titanium disulfide (TiS_2) is a group 4 TMD which debuted in the field of intercalation chemistry and batteries. Amongst the layered TMDs, it is recognised as a suitable cathode to pair with lithium anode due to high electronic conductivity, rapid lithium self-diffusion, stability, lightweight and low cost (Whittingham, 1976; Li et al., 2019). The material has also been promising for electrochemical (Lin et al., 2013; Toh et al.,

* Corresponding author. Center for Advanced Functional Nanorobots, Department of Inorganic Chemistry, University of Chemistry and Technology Prague, Czech Republic.
E-mail address: pumera.research@gmail.com (M. Pumera).

https://doi.org/10.1016/j.bios.2020.112114
Received 23 November 2019; Received in revised form 31 January 2020; Accepted 19 February 2020
Available online 22 February 2020

2016; Zeng et al., 2014) and thermoelectric (Imai et al., 2001; Wan et al., 2015) devices. Similar to its group 6 counterparts, MoS_2 and WS_2, structures and properties of TiS_2 can be tailored by doping. The introduction of foreign atoms or compositional variance would enhance its practicability in desired applications (Tan and Pumera, 2019). A variety of dopants has been incorporated into TiS_2, especially for thermoelectric applications to reduce thermal conductivity. They include alkali earth metals Mg (Qin et al., 2007; Putri et al., 2012), transition metals (Putri et al., 2013a) such as V, Nb, Ta (Beaumale et al., 2014a; Daou et al., 2015), Cr (Putri et al., 2013b), Mn, Fe, Co (Zhang et al., 2011), Ni (Zhang et al., 2006), Cu, Zn, Cd (Zhang et al., 2009) and even metalloids Ge (Hammoudi et al., 2019).

This paper embarks on the exploration of TiS_2 to unearth its electrochemical properties together with sensing capabilities. This is imperative because to date, there have been no electrochemical biosensors reported based on TiS_2 nor group 4 TMDs. Only group 6 TMDs are extensively studied for that matter, an example is previously reported MoS_2, $MoSe_2$, WS_2 and WSe_2 whose properties are modified by phase engineering (Rohaizad et al., 2017). Herein, doping is employed to enhance conductivity whose success hinges on the nature and concentration of dopant. TiS_2, being the parent compound, is doped with varying levels of Nb via controlled heating of elements in stoichiometric ratios. Nb is one of the most promising candidates as substitutional dopant since it is located in the adjacent group of Ti. The synthesised compounds are referred as $Ti_{1-x}Nb_xS_2$ where x = 0.05, 0.1, 0.2. Comparisons between group 4 Ti and group 5 Nb in the aspects of size, polymorph and valency would be drawn to elucidate the outcomes of conducted characterisation techniques. Fundamental electrochemical properties, particularly heterogeneous electron transfer and charge-transfer resistance, would be scrutinised together with their viability as a 2nd generation electrochemical biosensor for glucose detection.

2. Experimental section

2.1. Chemicals

Sulfur (99.999%), titanium (99%) and niobium powder (99.8%) were procured from STREM Chemicals. Sodium hydrogen phosphate (98+%), potassium dihydrogen phosphate (98+%) and potassium chloride (99%) were procured from Alfa Aesar. Ferrocenemethanol (>95%) was procured from Tokyo Chemical Industry. Potassium hexacyanoferrate (II) trihydrate (≥98.5%), potassium hexacyanoferrate (III) (~99%), glucose oxidase from Aspergillus niger (EC 1.1.3.4, type X-S), glutaraldehyde solution (50% in water), D-(+)-glucose (≥99.5%), L-ascorbic acid (BioXtra, ≥99.0%, crystalline), dopamine hydrochloride and uric acid (≥99%, crystalline) were procured from Sigma-Aldrich.

2.2. Preparation of Nb-Doped TiS_2

Titanium, niobium and sulfur were weighed in stoichiometric amounts, to a total of 10 g, and transferred into a quartz glass ampoule (30 × 130 mm; 1.5–2 mm wall thickness). The ampoule was evacuated to 5×10^{-5} mbar then melt-sealed by oxygen-hydrogen welding torch. Thereafter, it was placed in a muffle furnace and heated to 425 °C for 24 h. The temperature was adjusted to 500 °C over the next 24 h prior to the natural cooling of the ampoule to room temperature. Next, the ampoule was heated to 600 °C for 48 h, 800 °C for 48 h and lastly 850 °C for 12 h. The contents of the ampoule were mechanically mixed for 10 min before heating at the first two temperatures. Finally, the furnace was allowed to cool down naturally to ambient temperature. A ramping rate of 5 °C per minute was used throughout the synthesis.

2.3. Characterisation of materials

Samples for scanning electron microscopy (SEM) and X-ray photoelectron spectroscopy (XPS) were prepared by depositing a uniform thin layer of the solid compound onto a carbon-conductive tape. SEM with a field emission gun source (Tescan Lyra dual beam microscope) was operated to capture morphologies of the materials. XPS measurements relied on a Phoibos 100 spectrometer and a monochromatic Mg X-ray radiation source (SPECS, Germany). Wide survey as well as high-resolution spectra of Ti 2p, S 2p and Nb 3d were acquired. The data was processed with Casa XPS where peaks were calibrated with respect to carbon at 284.5 eV. Position, area and full width at half-maximum (fwhm) were constrained to obtain a good fitting during deconvolution. Raman spectroscopy was performed using an inVia Raman microscope (Renishaw, England) in backscattering mode with CCD detector, a 532 nm laser and 50x magnification objective lens. The instrument was calibrated according to silicon peak at 520 cm^{-1}. X-ray diffraction (XRD) was accomplished using Bruker D8 Discoverer (Bruker, Germany) with Cu Kα radiation source (λ = 0.15418 nm).

2.4. Preparation of biosensing electrodes

TiS_2 doped with varying amounts of Nb were suspended in ultrapure water, in concentrations of 5.0 and 7.5 mg mL^{-1} before and after optimisation respectively. They were ultrasonicated for three hours to attain a homogenous and well-dispersed suspension. Prior to the modification of the bare glassy carbon (GC) electrodes, they were polished with 0.5 and 0.05 μm alumina powder on a polishing pad. They were rinsed with ultrapure water before blown dry with N_2 gas. Subsequently, 3 μL of the suspension was drop casted onto a bare glassy carbon electrode, and left to dry. Once dried, 5 μL of glucose oxidase (GOx) in ultrapure water was successively drop casted, again left to dry in ambient conditions. 5 μL of 1% v/v glutaraldehyde (GTA) was drop casted as the final layer, and dried in oven at 35 °C for 30 min. The configuration of the biosensing electrode is referred as $Ti_{1-x}Nb_xS_2$/GOx/GTA and stored in the refrigerator at 4 °C overnight.

2.5. Electrochemical measurements

Electrochemical experiments were executed using Autolab PGSTAT204/FRA32 M (Eco Chemie, Utrecht, The Netherlands), controlled by Nova 1.10 software. A three electrode system was employed, comprising of bare or modified glassy carbon working electrode, platinum auxiliary/counter electrode and Ag/AgCl reference electrode. Heterogenous electron transfer (HET) rates of the materials were studied using cyclic voltammetry (CV) between the potentials of −1.0 and 1.0 V, at a scan rate of 100 mV s^{-1}. The redox probe, potassium hexacyanoferrate (10 mM) was prepared in supporting electrolyte potassium chloride (0.1 M).

The detection of glucose was performed based on $Ti_{1-x}Nb_xS_2$/GOx/GTA biosensing electrodes. Phosphate buffered saline (PBS) electrolyte was prepared by dissolving 0.356 g of potassium dihydrogen phosphate, 0.746 g of sodium hydrogen phosphate and 0.746 g of potassium chloride in 100 mL ultrapure water. The pH was adjusted to 7.20 by the addition of 1 M potassium hydroxide. Ferrocenemethanol (FcMeOH), mediator in the detection system, was prepared in concentration of 2 mM in PBS. In the chronoamperometric mode, the operating potential was set at 0.1 V. The current was allowed to stabilise for about 1000 s before introducing glucose into the solution. Baseline correction was performed to facilitate analysis and comparison.

3. Results and discussion

In this paper, we direct our focus to the effects of niobium (Nb) dopants on the structure and electrochemical sensing performance of titanium disulfide (TiS_2). Varying dopant concentrations were attained as $Ti_{1-x}Nb_xS_2$ (x = 0, 0.05, 0.1, 0.2) were synthesised by controlled heating of a sealed evacuated quartz glass ampoule, containing elements in stoichiometric ratios. Characterisation data obtained from scanning

electron microscopy (SEM), x-ray diffraction (XRD), Raman spectroscopy as well as x-ray photoelectron spectroscopy (XPS) would be presented and discussed herein. Heterogeneous electron transfer (HET), a key electrochemical parameter, would be compared across all four compounds followed by their capabilities to detect glucose in a 2nd generation electrochemical biosensor system (Scheme 1).

Fig. 1 presents morphologies of the synthesised compounds, captured at the same magnification using SEM. Pure TiS_2 exists as polygonal and thick multi-layered stacks. When doped with Nb, the structures seem to rupture and the layers become more obvious with increasing dopant concentration. The expansion of layers suggests Nb dopants, of larger ionic radii (0.68 Å), directly substituting Ti^{4+} (0.605 Å) in the lattice or intercalating amongst TiS_2 layers (Shannon, 1976). Additionally, a striking feature is noticed for $Ti_{0.8}Nb_{0.2}S_2$ where narrow and seemingly electron-transparent structures populate. These are described in literature as nanobelts (Hawkins and Whittaker-Brooks, 2018; Ma et al., 2006) or belt-like nanoribbons (Island et al., 2015).

While different morphologies are observed in SEM, Raman spectra demonstrate the same polymorphic structures for both pure and Nb-doped TiS_2 (Fig. 2A). The peaks at 235 and 332 cm^{-1} are assigned to E_g in-plane and A_{1g} out-of-plane vibrational modes accordingly. These two modes correspond to the 1T polymorph, also described by the D_{3d} ($P\bar{3}m1$) space group (Sandoval et al., 1991). It has been anticipated that the E_g mode will be of lower intensity than A_{1g} (Glebko et al., 2018). Moreover, there is a shoulder peak adjacent to A_{1g}, at approximately 370 cm^{-1}, characteristic of TiS_2 (Sandoval et al., 1992; Carmalt et al., 2004a). There are a few postulations to justify the presence of the shoulder peak, including a resonance effect which couple IR and Raman active modes or defects that lead to an excess of interlayer metal atoms (Sandoval et al., 1991; Sherrell et al., 2018). Overall, there are negligible changes in the Raman spectra with regards to peak positions and intensities. It can therefore be implied that the 1T polymorph is retained even after doping.

The acquired structural information from SEM and Raman spectroscopy is further supported by XRD (Fig. 2B). Consistent across our synthesised compounds, the first three, also dominant, peaks represent (001), (011) and (012) planes (Fig. 2B). They are indicative of 1T-TiS_2 (Lin et al., 2013), affirming the polymorph earlier deduced in Raman spectra. Meanwhile, the (001) peak stands out from the other two peaks with increasing dopant concentration. This implies a preferential orientation along the c axis that substantiates the layered structures observed in SEM. The primary cause could be the formation of TiS_3 nanobelts upon doping, since they tend to grow in the (001) direction (Island et al., 2015; Pawbake et al., 2015). Agreeably, TiS_3 peaks are identified in the XRD pattern of $Ti_{0.8}Nb_{0.2}S_2$and marked red.

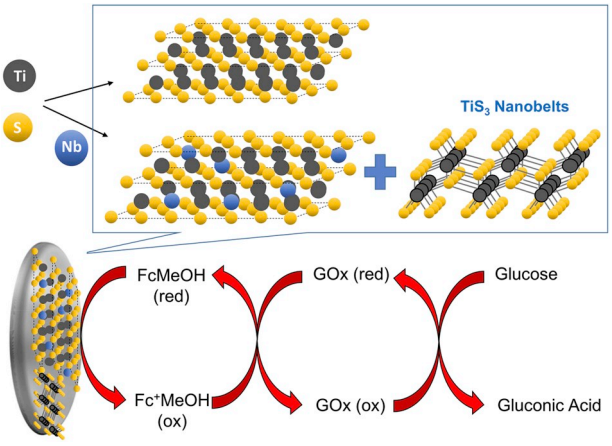

Scheme 1. Synthesis of layered 1T-TiS_2 together with TiS_3 nanobelts when doped. These materials are drop casted onto bare glassy carbon electrode for 2nd generation biosensor to detect glucose via enzymatic and mediator reactions.

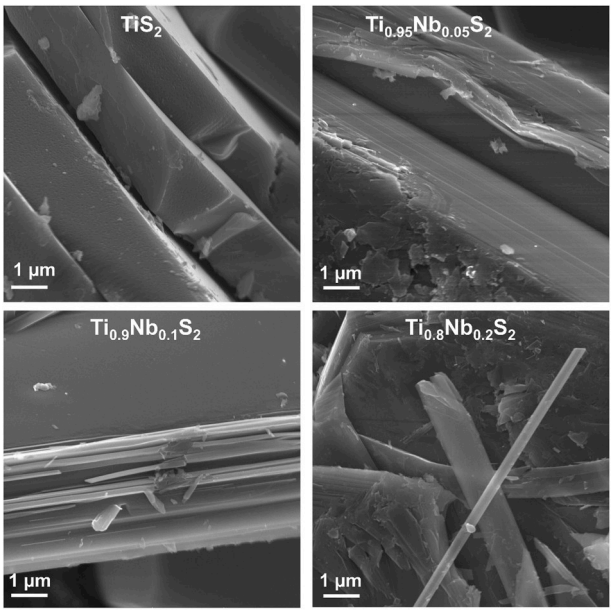

Fig. 1. Morphologies of pure TiS_2 together with its compounds of increasing dopant concentrations, captured by SEM.

XPS is useful to elucidate the chemical states upon doping. Zooming into the high resolution spectrum of Nb 3d region (Fig. 3A), the absence of dopants is ascertained for pure TiS_2. When Nb is introduced, deconvolution of the appeared peak reveals oxidation states of +2 and +5. Each state comes in a doublet where Nb (II) 3d 5/2 and 3/2 occur at 203.9 and 206.7 eV while Nb (V) 3d 5/2 and 3/2 at 206.7 and 209.4 eV. Although Nb (V) coincides with that of Nb_2O_5 (Mcguire et al., 1973), both of the states are prevalent for NbS_2 (Chia et al., 2016, 2018b) . This suggests a direct substitution of Nb atoms in TiS_2. If so, the coordination or polymorph has to be considered since TiS_2 and NbS_2 typically exist in 1T and 2H respectively. Nonetheless, it is possible that NbS_2 follows the polymorph of the host compound based on the obtained binding energies being close to values reported for 1T-NbS_2 (Carmalt et al., 2004b). The retention of 1T polymorph, regardless of dopant concentration studied, is in line with the previously discussed characterisation data. Additionally, a third pair of doublet is detected in HR-XPS spectra of $Ti_{0.9}Nb_{0.1}S_2$ and $Ti_{0.8}Nb_{0.2}S_2$ with higher dopant concentrations (x = 0.1, 0.2). They are assigned to Nb^{4+} species, where 3d5/2 and 3d3/2 possess binding energies of 205.2 and 207.9 eV respectively. A plausible explanation is Nb matching to the exclusive valency of Ti^{4+} in TiS_2 since valency is to be taken into account in substitutional doping. Isomorphic or isovalent substitution is desirable to preserve structural integrity and crystallinity.

The attention is subsequently turned to Ti 2p and S 2p regions to investigate the chemical states and more importantly, validate the relationship between Nb dopants with formation of TiS_3 nanobelts. Fig. 3B depicts Ti in its most stable +4 oxidation state, either as TiS_2, TiS_3 nanobelts or oxidised form TiO_2. The TiS_3 peaks can only be seen when doped, whose 2p3/2 peak is located at 456.4 eV. They are distinguishable from TiS_2 and TiO_2 whose 2p3/2 peaks are at 455.2 and 458.4 eV accordingly.

Likewise, the S 2p region reiterates the formation of TiS_3 nanobelts upon doping (Fig. S1). TiS_2 constitutes of only S^{2-} moieties whereas there are one S^{2-} and two S_2^{2-} for TiS_3 (Island et al., 2015; Fleet et al., 2005). As a result, there is an extra pair of doublet correlating to S_2^{2-} of TiS_3 upon doping. The S_2^{2-} 2p3/2 and 2p1/2 peaks at 161.1 and 162.3 eV intensifies with increasing dopant concentration. Because they are distinctly observed for $Ti_{0.9}Nb_{0.1}S_2$ and $Ti_{0.8}Nb_{0.2}S_2$, TiS_3 nanobelts are especially significant at higher dopant concentrations (x = 0.1, 0.2).

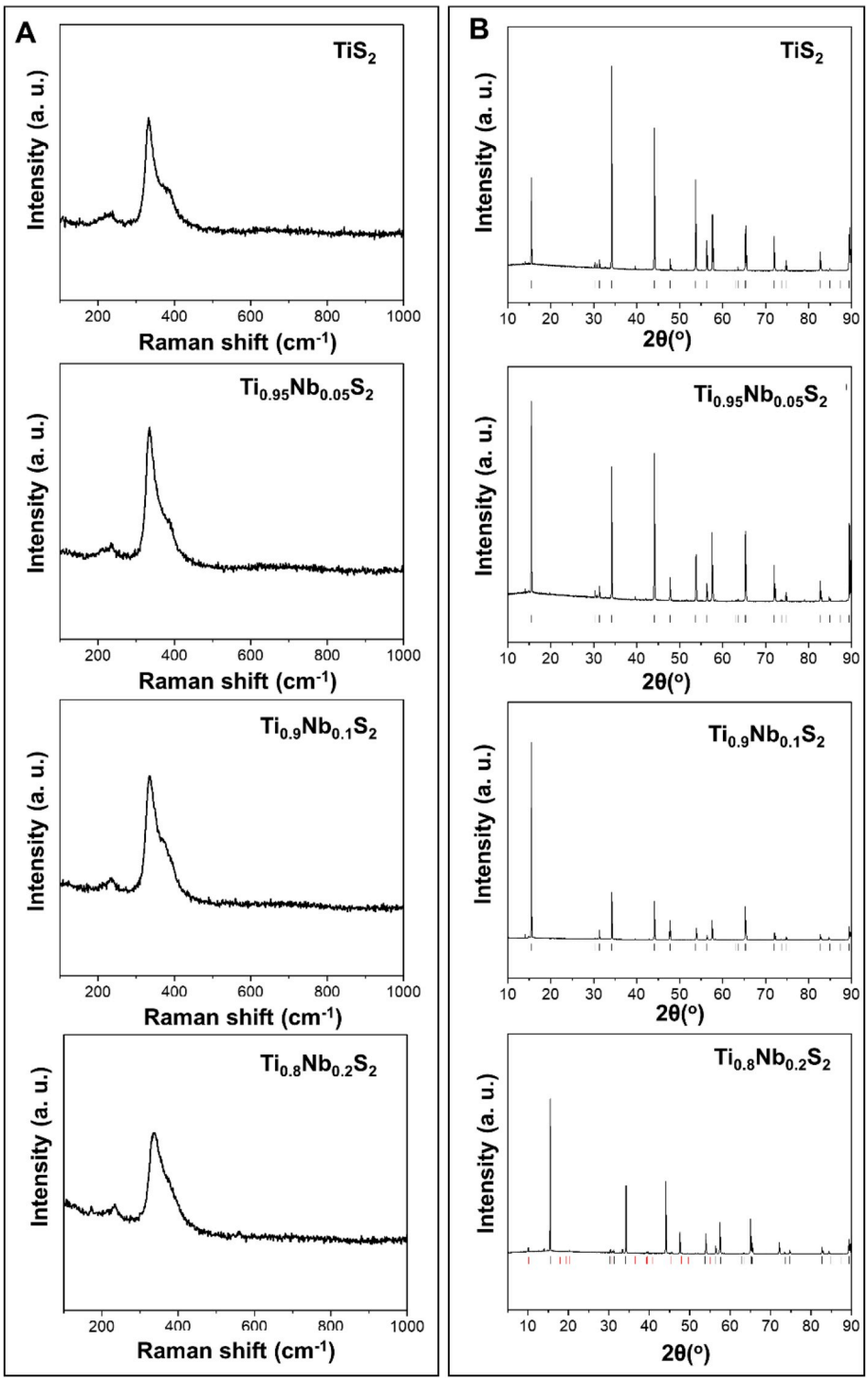

Fig. 2. Raman spectra (A) and X-ray diffraction pattern (B) of TiS_2, and its doped counterparts $Ti_{1-x}Nb_xS_2$ where x = 0.05), 0.1 and 0.2 (D).

The various characterisation techniques have put forth that doping TiS_2 with Nb atoms would result in TiS_3 nanobelts. The structural implications on the electrochemical properties of Nb-doped compounds would next be of interest. Suspensions of TiS_2 and the Nb-doped compounds are individually dropcasted onto bare glassy carbon (GC) electrodes while surface-sensitive ferro/ferricyanide redox probe is employed (Chen and Mccreery, 1996). Heterogenous electron transfer (HET) rates, impedance, electron transfer mechanism as well as electrochemically active area would be established. One of the key parameters is heterogeneous electron transfer (HET). A material is deemed suitable for electrochemical (bio)sensors if it promotes efficient electron transfer on the electrode surface, measured by small peak-to-peak separation (ΔE_p) in cyclic voltammograms (Nicholson, 1965). ΔE_p is extracted from the difference between oxidation and reduction peak potentials (Fig. S2A). It is the smallest for $Ti_{0.95}Nb_{0.05}S_2$, followed by TiS_2, $Ti_{0.9}Nb_{0.1}S_2$, then $Ti_{0.8}Nb_{0.2}S_2$ with the largest separation. Another observation is the appearance of anodic peaks at ~0.4 V specifically in the doped compounds. They grow intensely with increasing dopant concentration, unsurprisingly so as the peaks correspond to Nb oxidation from +4 to +5 (Chia et al., 2016). The oxidation is deemed as irreversible since there are no reduction peaks in response and would disappear in subsequent scans.

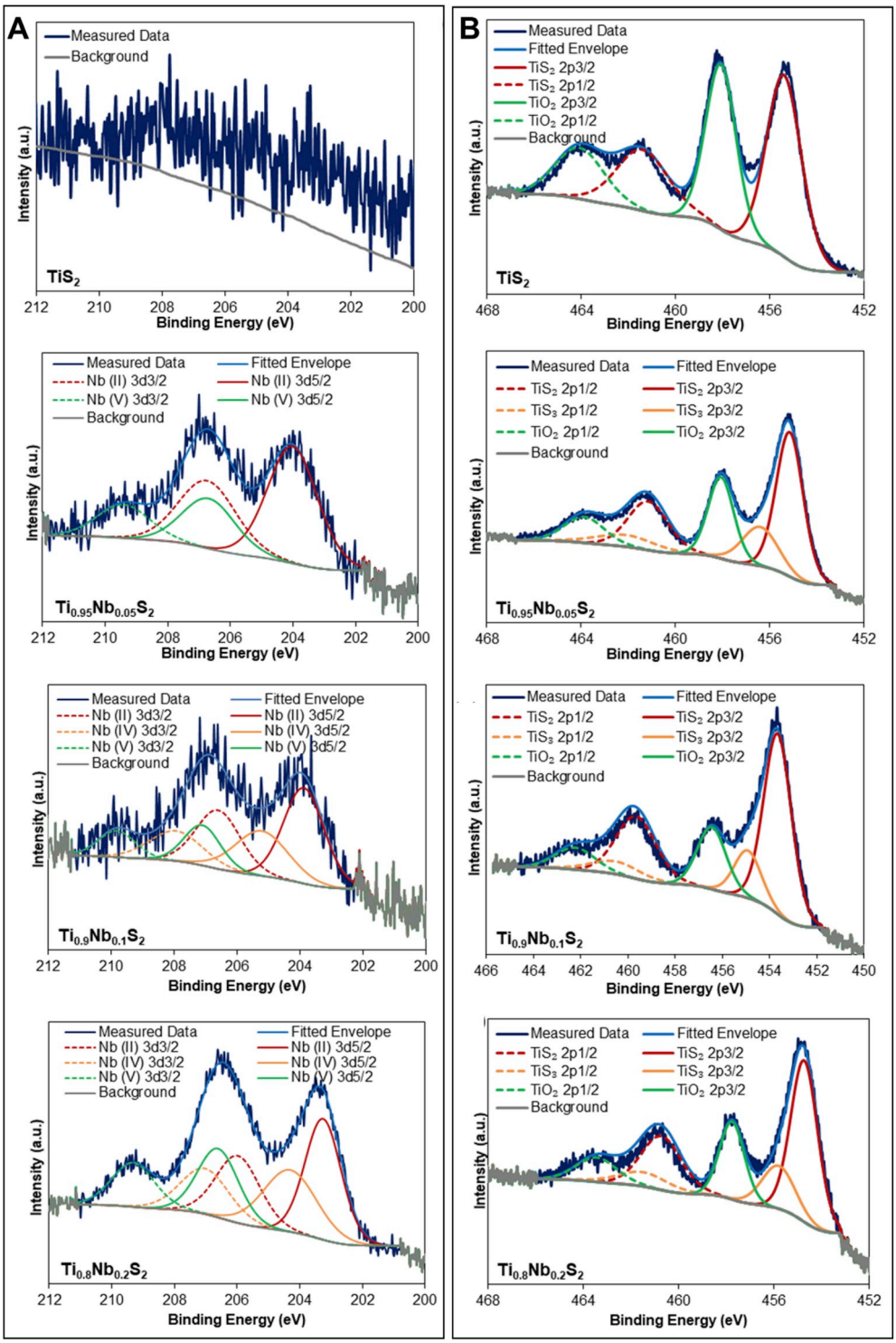

Fig. 3. Deconvoluted XPS spectra of (A) Nb 3d region showcasing the absence of Nb in pure TiS_2 and presence of Nb in doped compounds $Ti_{1-x}Nb_xS_2$ where x = 0.05, 0.1 and 0.2, and (B) Ti 2p region with stable Ti^{4+} oxidation state.

In the meantime, electrochemical impedance spectroscopy (EIS) was performed to probe fundamental properties of the materials. A graph of the imaginary part of the impedance (Z_i) versus the real part (Z_r), also termed as Nyquist plot, is displayed in Fig. S2B. The data is fitted using the Randles equivalent circuit to generate critical values, namely charge-transfer resistance (R_{ct}). R_{ct} is inversely proportional to electron transfer, henceforth smaller values are favoured. The materials are ranked in ascending R_{ct}, championed by $Ti_{0.95}Nb_{0.05}S_2$ (90 Ω) and trailing behind are TiS_2 (686 Ω), $Ti_{0.8}Nb_{0.2}S_2$ (800 Ω) then $Ti_{0.9}Nb_{0.1}S_2$ (1040 Ω).

Moving on, it is of interest to investigate the electron transfer mechanism of the $Ti_xNb_{1-x}S_2$ modified electrodes. The anodic peak current in the cyclic voltammetry of the ferro/ferricyanide redox probe is measured at different scan rates (Fig. S2C). A linear relationship between peak current and square root of scan rate in Fig. S2D indicates a diffusion-controlled process. The redox species is freely diffusing instead of adsorbed to the electrode surface. At the same time, the steepness of the slopes differ across compounds and the modified working electrode

area can be determined. By relying on the Randles-Sevcik equation, known values of diffusion coefficient ($D = 7.26 \times 10^{-6}$ cm^2 s^{-1}) and concentration ($C = 10 \times 10^{-6}$ mol cm^{-3}) of the redox probe are substituted. The electrochemically active areas are calculated to be 0.024, 0.041, 0.023 and 0.022 cm^2 for TiS_2, $Ti_{0.95}Nb_{0.05}S_2$, $Ti_{0.9}Nb_{0.1}S_2$ and $Ti_{0.8}Nb_{0.2}S_2$ respectively. It is the largest for $Ti_{0.95}Nb_{0.05}S_2$.

Combining efficient electron transfer rates, low resistance and large electrochemically active area, doping TiS_2 with a specific concentration of Nb dopants has successfully enhanced electrochemical properties. This in agreement with another study which reported an increase in electrical conductivity of Nb-doped TiS_2 (Beaumale et al., 2014b). Putting forth that Nb is more electron rich, d^1 in Nb^{4+} compared to d^0 in Ti^{4+}, there would be an increase in electron concentration. Since the principle valence band is full in TiS_2, additional electrons from Nb would partially fill the conduction band. Electrical conductivity consequently increases therefore superior electrochemical sensing performances are anticipated for $Ti_{0.95}Nb_{0.05}S_2$.

Pure and Nb-doped TiS_2 are put to the test where they would be coupled with glucose oxidase enzyme (GOx) and glutaraldehyde (GTA). GTA is selected due to its high reactivity and desired stability, apart from being a simple and gentle cross-linking agent (Migneault et al., 2004; Barbosa et al., 2014). The efficiency of GTA is demonstrated by several enzymatic-based biosensor previously reported by our group (Mayorga-Martinez et al., 2019a, 2019b; Nasir et al., 2017; Rohaizad et al., 2017; Toh et al., 2017) and others too (Albareda-Sirvent et al., 2000; Lei and Deng, 1996; Li et al., 1999; Cardoso et al., 2020). Drop-casted component-by-component onto bare GC electrodes, the prepared biosensing electrodes would be placed in an electrochemical system to detect glucose. The series of chemical events are deconstructed in the following equations. While processing glucose, the flavin redox center (FAD) of GOx is reduced. Regeneration of the oxidised form is necessary and facilitated by ferrocenemethanol (FcMeOH). The ferrocene-derivative plays the role of a mediator, whose oxidation at the electrode surface is quantifiable and proportional to glucose levels (Bourdillon et al., 1995). The involvement of the mediator renders the electrochemical biosensor as 2nd generation.

$$\text{Glucose} + \text{FAD-GOx} + \tfrac{1}{2}\,O_2 \rightarrow \text{Gluconic acid} + \text{FADH}_2\text{-GOx} + H_2O_2 \quad (1)$$

$$\text{FADH}_2\text{-GOx} + 2\,Fc^{+}\text{MeOH} \rightarrow \text{FAD-GOx} + 2\,\text{FcMeOH} + 2\,H^{+} \quad (2)$$

$$2\ \text{FcMeOH} \xrightarrow[100\ \text{mV}]{\text{Ti}_{1-x}\text{Nb}_x\text{S}_2} 2\,Fc^{+}\text{MeOH} + 2\,e^{-} \quad (3)$$

Pure and Nb-doped TiS_2 were incorporated on the electrode surface as an attempt to enhance the signal transduction for glucose detection. Fig. 4A displays the cyclic voltammograms of FcMeOH upon addition of 1 mM glucose for the respective $Ti_{1-x}Nb_xS_2$/GOx/GTA biosensing electrodes. Instead of the typical pair of reversible redox peaks, the peaks are asymmetric where the anodic peak current is of significantly higher intensity than the cathodic. This implies successful detection of glucose since oxidation of FcMeOH has occurred, a product of enzyme regeneration following the mechanism. Among the materials, $Ti_{0.95}Nb_{0.05}S_2$ generates the largest oxidation peak. Its high sensitivity is evident in chronoamperometry experiments where distinctly large current response is achieved (Fig. 4B). In contrast, $Ti_{0.9}Nb_{0.1}S_2$ and $Ti_{0.8}Nb_{0.2}S_2$ produce comparable responses to pure TiS_2. A high dopant concentration of Nb ($x = 0.1, 0.2$) impedes the electrochemical performance due to the formation of TiS_3 nanobelts based on previously discussed characterisation data. Doping would therefore only improve biosensing capabilities at specific dopant concentrations. As the best performing material, subsequent experiments are modelled with $Ti_{0.95}Nb_{0.05}S_2$/GOx/GTA electrodes.

The current response grew with increasing drop-cast concentration (Fig. 4C). Loading more $Ti_{0.95}Nb_{0.05}S_2$ on the electrode surface emphasises its role in enhancing signal transduction. Meanwhile, the role of other components are investigated by manipulating configurations of the biosensing electrode (Fig. 4D). No current response is observed for bare GC and $Ti_{0.95}Nb_{0.05}S_2$ electrode, until integrated with GOx. The enzyme is imperative in recognising glucose and triggering the detection

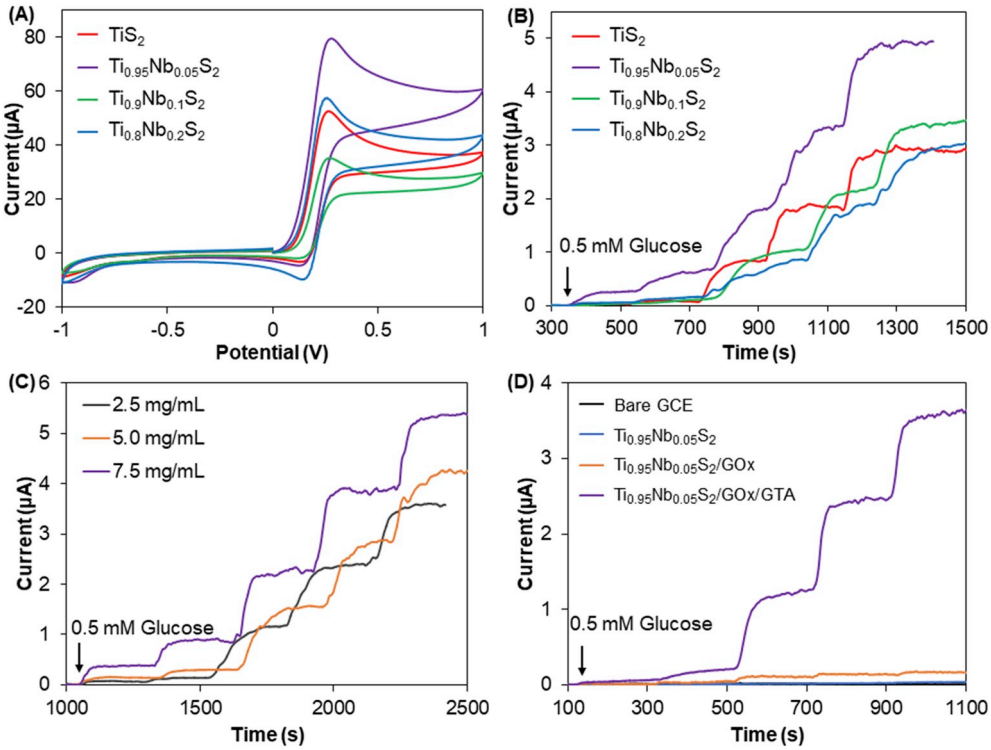

Fig. 4. Current responses of biosensing electrodes ($Ti_{1-x}Nb_xS_2$/GOx/GTA) in cyclic voltammograms at 100 mV s^{-1} scan rate (A), and chronoamperometry data (B) upon addition of 1 mM and 0.5 mM glucose respectively. Chronoamperometry data of $Ti_{0.95}Nb_{0.05}S_2$/GOx/GTA biosensing electrode when varying drop-cast concentrations (C) and configurations (D). Conditions: 2 mM FcMeOH in PBS pH 7.20 electrolyte.

mechanism. The current response dramatically increases when GTA is added, an effective cross-linker to stabilise the modified biosensor by keeping the layers intact for reliable glucose measurements.

The aforementioned experiments were carried out at the potential of 0.1 V. Nevertheless, adjustment of the operating potential is necessary if selectivity is not fulfilled. Signals from electrochemically active interferences should be minimised, namely ascorbic acid (AA), dopamine (DA) and uric acid (UA). They are known to be in concentrations 30 times lower than glucose in blood (Bourdillon et al., 1995), hence 0.2 mM was added in relation to 5 mM glucose. In Fig. 5A, increasing operating potentials generates higher current responses for glucose as well as interferences, unfortunately. Fig. 5B then compares the responses of the interferences as a percentage of glucose for the different potentials studied. At 0.1 V, the signals from interferences fall below 15% of glucose unlike 0.15 and 0.2 V. Although a higher potential is desired for a more sensitive biosensor, selectivity is another critical criterion that should not be compromised. Operating potential of 0.1 V is maintained since both sensitivity and selectivity are satisfactory.

With all the critical parameters optimised for the $Ti_{0.95}Nb_{0.05}S_2$-based biosensor, its analytical performance is evaluated. Four different glucose concentrations were prepared (5, 50, 500 and 5000 μM) and each added five times into the measured solution sequentially. No current response is acquired during the addition of 5 μM, but a stepwise increase in current is observed with higher concentrations thereafter (Fig. 5C). To ensure the repeatability of the developed biosensor, triplicates of the experiment yield a relative standard deviation percentage of 11.7%. A calibration graph of current against glucose concentration was then plotted (Fig. 5D). Three linear ranges are obtained, 74.6–272.9 μM (r = 0.995), 0.767–12.6 mM (r = 0.995) and 17.5–27.3 mM (r = 0.990). A sensitivity of 17.9 μA mM^{-1} cm^{-2} is determined based on the electrochemically active area. The limit of detection and quantification are computed to be 25.7 μM and 85.7 μM respectively. The stability of the biosensor is also emphasised as the measurement was performed over a long duration of 4500 s (75 min) yet glucose was quantified reliably and precisely with low standard deviation.

The developed $Ti_{0.95}Nb_{0.05}S_2$-based biosensor was put to the test to detect glucose in real sample. Instead of adding prepared concentration of glucose into the solution, human serum procured from Sigma-Aldrich was directly injected. A current response is attained and 2.68 ± 0.55 mM (n = 3) of glucose was quantified after extrapolation from calibration graph and considering the dilution factor. The detected concentration falls short from the specified range of 3.33–7.78 mM. Stability of the developed biosensor was also scrutinised over a period of five days. The current responses upon addition of 0.5 mM glucose were expressed as percentage recovery with respect to day 1. The percentage dropped to 86% in day 3 then relatively maintained to 83% in day 5 (Fig. S3). Finally, other glucose biosensors based on TMDs and other layered materials are compared. Their linear ranges, sensitivities and limit of detections are compiled in Table 1. Examining the parameters of the biosensors, $Ti_{0.95}Nb_{0.05}S_2$-based exhibit wide linear ranges from μM to mM and highest sensitivity.

4. Conclusion

TiS_2 has been successfully doped with Nb, $Ti_{1-x}Nb_xS_2$, and we aimed to study the doping outcomes influenced by nature as well as concentration of dopants (x = 0.05, 0.1, 0.2). Characterisation data from various techniques validate the synthesis of TiS_2 and bring to light the changes in its structure upon doping. Aspects of size, polymorph and valency are included in the discussion. The 1T polymorph is retained across all dopant concentrations, however TiS_3 nanobelts are formed especially at higher concentration of x = 0.2. With the structural effects in mind, fundamental electrochemical properties of the materials were compared. $Ti_{0.95}Nb_{0.05}S_2$ demonstrated largest electrochemically active area, superior conductivity and least resistance to electron transfer based on HET and impedance studies. When applied in glucose detection, $Ti_{0.95}Nb_{0.05}S_2$ generated the highest response. A sensitive and selective 2nd generation electrochemical biosensor is developed based on $Ti_{0.95}Nb_{0.05}S_2$/GOx/GTA. The linear ranges are 74.6–272.9 μM (r = 0.995), 0.767to 12.6 mM (r = 0.995) and 17.5–27.3 mM (r = 0.990), while 25.7 μM and 85.7 μM are achieved as the limit of detection and quantification respectively. Electrochemical properties and sensing capabilities have been enhanced by doping TiS_2 with a specific concentration of Nb. Higher concentrations would result in structural

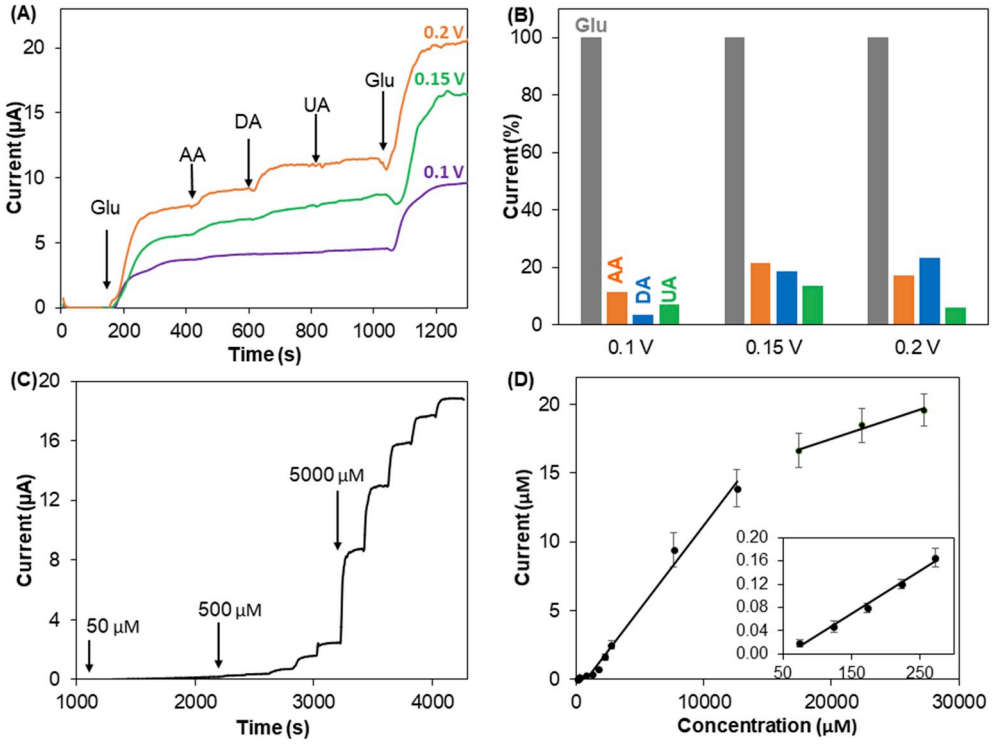

Fig. 5. Chronoamperometry data upon successive additions of 5 mM glucose and 0.2 mM interferences at different operating potentials (A), followed by comparison of current signals from interferences as a percentage of glucose (B). Chronoamperometry data when introducing 50, 500 and 5000 μM glucose in the solution, each concentration added 5 times (C), along with calibration graph of current against glucose concentration with three linear ranges, smallest range is displayed as inset (D). Conditions: $Ti_{0.95}Nb_{0.05}S_2$/GOx/GTA biosensing electrode, 2 mM FcMeOH in PBS pH 7.20 electrolyte.

Table 1
Representative glucose biosensors based on layered materials in literature: comparison of linear range, sensitivity and limit of detection (LOD).

Material	Biosensor Architecture (Generation)	Linear Range	Sensitivity	LOD (μM)	Ref
$Ti_{0.95}Nb_{0.05}S_2$	GCE/$Ti_{0.95}Nb_{0.05}S_2$/GOx/GTA (2nd Gen)	74.6–272.9 μM 0.767–12.6 mM 17.5–27.3 mM	17.9 μA mM^{-1} cm^{-2}	25.7	This work
MoS_2	AuE/AuNP–MoS_2/GOx (2nd Gen)	0.25–13.2 mM	13.8 μA μM^{-1} cm^{-2}	0.042	Parlak et al. (2017)
1T-WS_2	GCE/1T-WS_2/GOx/GTA (2nd Gen)	176–766 μM 1.3–22.3 mM	–	82.6	Rohaizad et al. (2017)
$Ti_3C_2T_x$	GCE/Au–$Ti_3C_2T_x$/GOx/Nafion (1st Gen)	0.1–18 mM	4.2 μA mM^{-1} cm^{-2}	5.9	Rakhi et al. (2016)
$Ti_3C_2T_x$	GCE/$Ti_3C_2T_x$-Graphene/GOx/Nafion (1st Gen)	0.2–5.5 mM	12.10 μA mM^{-1}	100	Gu et al. (2019)

implications of TiS_3 nanobelts which may impede performance.

Declaration of competing interest

The authors declare that they have no known competing financial interests or personal relationships that could have appeared to influence the work reported in this paper.

CRediT authorship contribution statement

Nasuha Rohaizad: Investigation, Visualization, Formal analysis, Writing - original draft. **Carmen C. Mayorga-Martinez:** Conceptualization, Formal analysis, Writing - review & editing. **Zdeněk Sofer:** Resources, Formal analysis, Writing - review & editing. **Richard D. Webster:** Project administration, Formal analysis, Writing - review & editing. **Martin Pumera:** Supervision, Formal analysis, Writing - review & editing.

Acknowledgements

M.P. acknowledges the financial support of Grant Agency of the Czech Republic (EXPRO: 19-26896X).

Appendix A. Supplementary data

Supplementary data to this article can be found online at https://doi.org/10.1016/j.bios.2020.112114.

References

Albareda-Sirvent, M., Merkoci, A., Alegret, S., 2000. Sens. Actuators, B 69, 153–163.
Barbosa, O., Ortiz, C., Berenguer-Murcia, Á., Torres, R., Rodrigues, R.C., Fernandez-Lafuente, R., 2014. RSC Adv. 4, 1583–1600.
Beaumale, M., Barbier, T., Bréard, Y., Hébert, S., Kinemuchi, Y., Guilmeau, E., 2014a. J. Appl. Phys. 115, 043704.
Beaumale, M., Barbier, T., Bréard, Y., Raveau, B., Kinemuchi, Y., Funahashi, R., Guilmeau, E., 2014b. J. Electron. Mater. 43, 1590–1596.
Bourdillon, C., Demaille, C., Moiroux, J., Saveant, J.-M., 1995. J. Am. Chem. Soc. 117, 11499–11506.
Cardoso, R.M., Silva, P.R., Lima, A.P., Rocha, D.P., Oliveira, T.C., do Prado, T.M., Muñoz, R.A., 2020. Sens. Actuators, B 307, 127621.
Carmalt, C.J., Oneill, S.A., Parkin, I.P., Peters, E.S., 2004a. J. Mater. Chem. 14, 830.
Carmalt, C.J., Manning, T.D., Parkin, I.P., Peters, E.S., Hector, A.L., 2004b. J. Mater. Chem. 14, 290.
Chen, P., Mccreery, R.L., 1996. Anal. Chem. 68, 3958–3965.
Cheng, R., Jiang, S., Chen, Y., Liu, Y., Weiss, N., Cheng, H.-C., Wu, H., Huang, Y., Duan, X., 2014. Nat. Commun. 5, 5143.
Chhowalla, M., Shin, H.S., Eda, G., Li, L.-J., Loh, K.P., Zhang, H., 2013. Nat. Chem. 5, 263–275.
Chia, X., Pumera, M., 2018. Chem. Soc. Rev. 47, 5602–5613.
Chia, X., Ambrosi, A., Lazar, P., Sofer, Z., Pumera, M., 2016. J. Mater. Chem. A 4, 14241–14253.
Chia, X., Sutrisnoh, N.A.A., Sofer, Z., Luxa, J., Pumera, M., 2018. Chem. Eur J. 24, 3199–3208.
Daou, R., Takahashi, H., Hébert, S., Beaumale, M., Guilmeau, E., Maignan, A., 2015. J. Appl. Phys. 117, 165101.
Ferrari, A.C., Bonaccorso, F., Fal'Ko, V., Novoselov, K.S., Roche, S., Bøggild, P., Borini, S., Koppens, F.H., Palermo, V., Pugno, N., Garrido, J.A., 2015. Nanoscale 7, 4598–4810.
Fleet, M., Harmer, S., Liu, X., Nesbitt, H., 2005. Surf. Sci. 584, 133–145.
Geim, A.K., Novoselov, K.S., 2007. Nat. Mater. 6, 183–191.
Glebko, N., Aleksandrova, I., Tewari, G.C., Tripathi, T.S., Karppinen, M., Karttunen, A., 2018. J. Phys. Chem. C 122, 26835–26844.
Gu, H., Xing, Y., Xiong, P., Tang, H., Li, C., Chen, S., Zeng, R., Han, K., Shi, G., 2019. ACS Appl. Nano Mater. 2, 6537–6545.
Hammoudi, L., Gómez-Herrero, A., Kars, M., Roisnel, T., Otero-Diáz, L.C., 2019. C. R. Chim. 22, 406–418.
Hawkins, C.G., Whittaker-Brooks, L., 2018. ACS Appl. Nano Mater. 1, 851–859.
Higgins, T.M., Finn, S., Matthiesen, M., Grieger, S., Synnatschke, K., Brohmann, M., Rother, M., Backes, C., Zaumseil, 2018. Adv. Funct. Mater. 1804387.
Hu, G., Kang, J., Ng, L.W.T., Zhu, X., Howe, R.C.T., Jones, C.G., Hersam, M.C., Hasan, T., 2018. Chem. Soc. Rev. 47, 3265–3300.
Imai, H., Shimakawa, Y., Kubo, Y., 2001. Phys. Rev. B 64, 241104.
Island, J.O., Barawi, M., Biele, R., Almazán, A., Clamagirand, J.M., Ares, J.R., Sánchez, C., Van Der Zant, Herre S.J., Álvarez, J.V., Dagosta, R., Ferrer, I.J., Castellanos-Gomez, A., 2015. Adv. Mater. 27, 2595–2601.
Lei, C., Deng, J., 1996. Anal. Chem. 68, 3344–3349.
Li, Y.G., Zhou, Y.X., Feng, J.L., Jiang, Z.H., Ma, L.R., 1999. Anal. Chim. Acta 382, 277–282.
Li, L., Li, Z., Yoshimura, A., Sun, C., Wang, T., Chen, Y., Chen, Z., Littlejohn, A., Xiang, Y., Hundekar, P., Bartolucci, S.F., Shi, J., Shi, S.-F., Meunier, V., Wang, G.-C., Koratkar, N., 2019. Nat. Commun. 10, 1764.
Lin, C., Zhu, X., Feng, J., Wu, C., Hu, S., Peng, J., Guo, Y., Peng, L., Zhao, J., Huang, J., Yang, J., Xie, Y., 2013. J. Am. Chem. Soc. 135, 5144–5151.
Luo, P., Zhuge, F., Zhang, Q., Chen, Y., Lv, L., Huang, Y., Li, H., Zhai, T., 2019. Nanoscale Horiz. 4, 26–51.
Ma, J., Liu, X., Cao, X., Feng, S., Fleet, M.E., 2006. Eur. J. Inorg. Chem. 2006, 519–522.
Mayorga-Martinez, C.C., Gusmão, R., Sofer, Z., Pumera, M., 2019a. Angew. Chem. Int. Ed. 58, 134–138.
Mayorga-Martinez, C.C., Sofer, Z., Pumera, M., 2019b. ACS Nano 13, 13217–13224.
Mcguire, G.E., Schweitzer, G.K., Carlson, T.A., 1973. Inorg. Chem. 12, 2450–2453.
Mcmanus, D., Vranic, S., Withers, F., Sanchez-Romaguera, V., Macucci, M., Yang, H., Sorrentino, R., Parvez, K., Son, S.-K., Iannaccone, G., Kostarelos, K., Fiori, G., Casiraghi, C., 2017. Nat. Nanotechnol. 12, 343–350.
Migneault, I., Dartiguenave, C., Bertrand, M.J., Waldron, K.C., 2004. Biotechniques 37, 790–802.
Moving towards the market. Nat. Mater. 18, 2019, 519.
Nasir, M.Z.M., Mayorga-Martinez, C.C., Sofer, Z., Pumera, M., 2017. ACS Nano 11, 5774–5784.
Nicholson, R.S., 1965. Anal. Chem. 37, 1351–1355.
Novoselov, K.S., 2004. Science 306, 666–669.
Parlak, O., İncel, A., Uzun, L., Turner, A.P., Tiwari, A., 2017. Biosens. Bioelectron. 89, 545–550.
Pawbake, A.S., Island, J.O., Flores, E., Ares, J.R., Sanchez, C., Ferrer, I.J., Jadkar, S.R., Van Der Zant, Herre S.J., Castellanos-Gomez, A., Late, D.J., 2015. ACS Appl. Mater. Interfaces 7, 24185–24190.
Putri, Y.E., Wan, C., Wang, Y., Norimatsu, W., Kusunoki, M., Koumoto, K., 2012. Scripta Mater. 66, 895–898.
Putri, Y.E., Wan, C., Dang, F., Mori, T., Ozawa, Y., Norimatsu, W., Kusunoki, M., Koumoto, K., 2013a. J. Electron. Mater. 43, 1870–1874.
Putri, Y.E., Wan, C., Zhang, R., Mori, T., Koumoto, K., 2013b. J. Adv. Ceram. 2, 42–48.
Qin, X.Y., Zhang, J., Li, D., Dong, H.Z., Wang, L., 2007. J. Appl. Phys. 102, 073703.
Rakhi, R.B., Nayak, P., Xia, C., Alshareef, H.N., 2016. Sci. Rep. 6, 1–10.
Rohaizad, N., Mayorga-Martinez, C.C., Sofer, Z., Pumera, M., 2017. ACS Appl. Mater. Interfaces 9, 40697–40706.
Rowley-Neale, S.J., Smith, G.C., Banks, C.E., 2017. ACS Appl. Mater. Interfaces 9, 22539–22548.
Sandoval, S.J., Yang, D., Frindt, R.F., Irwin, J.C., 1991. Phys. Rev. B 44, 3955–3962.
Sandoval, S.J., Chen, X.K., Irwin, J.C., 1992. Phys. Rev. B 45, 14347–14353.
Shannon, R.D., 1976. Acta Crystallogr. A 32, 751–767.
Sherrell, P.C., Sharda, K., Grotta, C., Ranalli, J., Sokolikova, M.S., Pesci, F.M., Palczynski, P., Bemmer, V.L., Mattevi, C., 2018. ACS Omega 3, 8655–8662.
Singh, E., Singh, P., Kim, K.S., Yeom, G.Y., Nalwa, H.S., 2019. ACS Appl. Mater. Interfaces 11, 11061–11105.
Tan, S.M., Pumera, M., 2019. ACS Nano 13, 2681–2728.
Tedstone, A.A., Lewis, D.J., O'Brien, P., 2016. Chem. Mater. 28, 1965–1974.
Toh, R.J., Sofer, Z., Pumera, M., 2016. J. Mater. Chem. A 4, 18322–18334.
Toh, R.J., Mayorga-Martinez, C.C., Sofer, Z., Pumera, M., 2017. Adv. Funct. Mater. 27, 1604923.
Velusamy, D.B., Kim, R.H., Cha, S., Huh, J., Khazaeinezhad, R., Kassani, S.H., Song, G., Cho, S.M., Cho, S.H., Hwang, I., Lee, J., Oh, K., Choi, H., Park, C., 2015. Nat. Commun. 6, 8063.

Wan, C., Gu, X., Dang, F., Itoh, T., Wang, Y., Sasaki, H., Kondo, M., Koga, K., Yabuki, K., Snyder, G.J., Yang, R., Koumoto, K., 2015. Nat. Mater. 14, 622–627.
Whittingham, M.S., 1976. Science 192, 1126–1127.
Wilson, J., Yoffe, A., 1969. Adv. Phys. 18, 193–335.
Zeng, Z., Tan, C., Huang, X., Bao, S., Zhang, H., 2014. Energy Environ. Sci. 7, 797–803, 2014.
Zhang, J., Qin, X.Y., Li, D., Dong, H.Z.J., 2006. Phys. D: Appl. Phys. 39, 1230–1236.
Zhang, J., Qin, X.Y., Li, D., Xin, H.X., Pan, L., Zhang, K.X., 2009. J. Alloys Compd. 479, 816–820.
Zhang, J., Qin, X.Y., Xin, H.X., Li, D., Song, C.J., 2011. J. Electron. Mater. 40, 980–986.
Zhang, P., Yang, S., Pineda-Gómez, R., Ibarlucea, B., Ma, J., Lohe, M.R., Akbar, T.F., Baraban, L., Cuniberti, G., Feng, X., 2019. Small 15, 1901265.